Since January 2020 Elsevier has created a COVID-19 resource centre with free information in English and Mandarin on the novel coronavirus COVID-19. The COVID-19 resource centre is hosted on Elsevier Connect, the company's public news and information website.

Chemical Data Collections 17–18 (2018) 236–250

Contents lists available at ScienceDirect

Chemical Data Collections

journal homepage: www.elsevier.com/locate/cdc

Spectroscopic (FT-IR, FT-Raman) investigation, topology (ESP, ELF, LOL) analyses, charge transfer excitation and molecular docking (dengue, HCV) studies on ribavirin

Fathima Rizwana B.[a], S. Muthu[b,*], Johanan Christian Prasana[a], Christina Susan Abraham[a], M. Raja[c]

[a] Department of Physics, Madras Christian College, Chennai 600059 Tamil Nadu, India
[b] Department of Physics, Arignar Anna Government Arts College, Cheyyar 604407 Tamil Nadu, India
[c] Department of Physics, Government Thirumagal Mills College, Vellore 635803 Tamil Nadu, India

ARTICLE INFO

Article history:
Received 27 June 2018
Revised 2 September 2018
Accepted 10 September 2018
Available online 15 September 2018

Keywords:
DFT
FT-IR
ESP
Charge transfer excitation
Molecular docking

ABSTRACT

Ribavirin, a triazole derivative has a wide application in the medical field as an antiviral drug. In the present work, a quantum chemical approach was followed to study the vibrational modes and the reactivity. Experimental techniques of FT-IR, FT-Raman were used to study the vibrational spectrum. A complete vibrational analysis was carried out and assignments of the fundamental modes were proposed. Molecular electrostatic potential, frontier molecular orbitals, electronic localization function and fukui functions were analyzed by using wavefunction analyser, Multiwfn 3.4.1 to study the chemical reactivity. Band gap energy of the title molecule is found to be 6.01 eV, as calculated from the HOMO-LUMO energies. The intermolecular charge transfer within the molecule was confirmed from the charge transfer interactions. Molecular docking studies were carried out to study the biological activity of the compound. Viral target proteins such as Dengue and Hepatitis C were chosen and the respective docking parameters were calculated.

Specifications table

Subject area	Spectroscopy and Computational Chemistry
Compounds	Ribavirin
Data category	Spectral, computational simulations and molecular docking.
Data acquisition format	FT-IR, FT-Raman
Data type	Experimental and theoretical
Procedure	The title compound was purchased in its pure form and the experimental and computational methods were carried out to characterize and study the reactivity of the compound to a couple of proteins.
Data accessibility	Data is within the article

1. Rationale

Owing to their interesting physiological properties, a decent number of five membered aromatic systems having three heteroatoms at symmetrical positions have been studied. The presence of three nitrogens in triazole provides an interesting

* Corresponding author.
E-mail address: mutgee@gmail.com (S. Muthu).

https://doi.org/10.1016/j.cdc.2018.09.003
2405-8300/

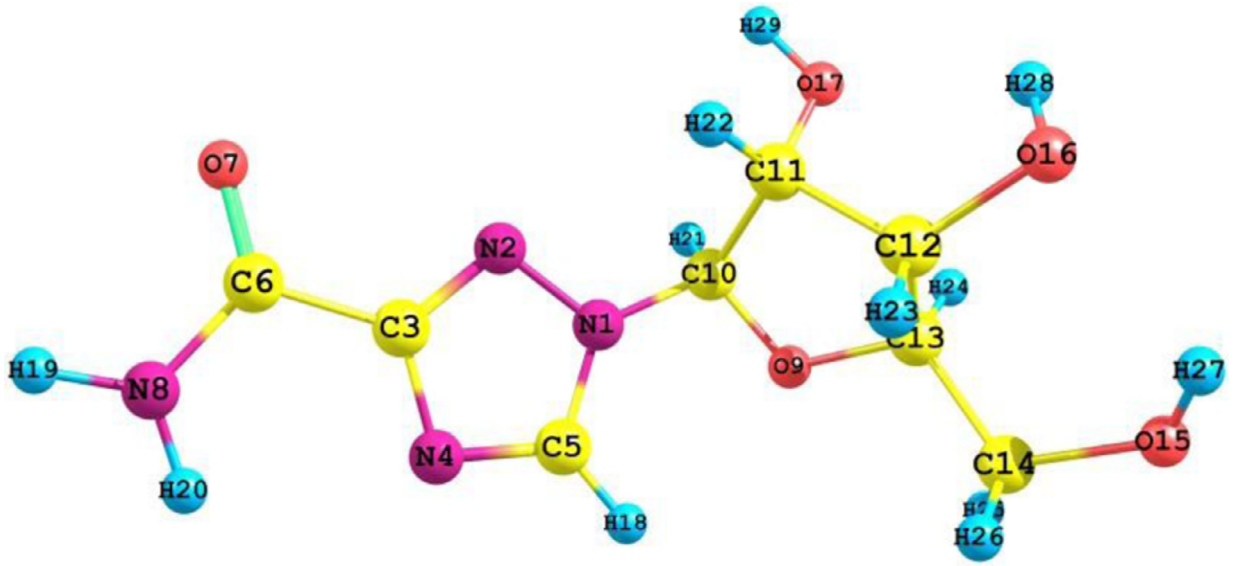

Fig. 1. Optimized geometric structure with atom numbering of the title compound.

class of compounds. Triazole and its derivatives exhibit a broad spectrum of pharmacological properties such as antibacterial and antifungal activities [1] and also there are a lot of reports on the interaction between triazole and metal in preventing corrosion of metals [2–5]. Although triazole and its derivatives show a wide spectrum of activity, the literature search revealed that not much has been reported about the structure/activity relationship of this class of compounds. An ab-initio method has been followed to study the derivatives of triazoles [6–8]. Since the first report of the broad spectrum antiviral activity and synthesis of ribavirin [9,10], the in vitro and in vivo antiviral activity has been confirmed in many independent laboratories [11–17]. Ribavirin has been proved clinically effective against hepatitis A virus [18–20]. Synthesis and determination of antiviral activity of the 2′(3′)-O-Methyl derivatives of Ribavirin [21], of some phosphates of ribavirin [22] and amino acid esters of ribavirin were discussed in detail [23].

To the best of our knowledge, no detailed spectroscopic investigation has been made on the title compound. This motivates to provide a complete vibrational spectroscopic investigation on the molecule to give a detailed assignment of the fundamental bands in FTIR and FT Raman spectra on the basis of calculated PED. The present study provides a complete vibrational and electronic analysis under both theoretical and experimental background. A complete spectroscopic investigation of the title compound using B3LYP/6–311++G(d,p) level of the theory has been reported in this work. In this attempt, the vibrational analysis has been performed to screen the physical and chemical properties of the present compound using computational calculations using Density Functional Theory. The distribution of electrons and the reactive sites on the surface of the title compound were analysed using ESP (Electrostatic potential), ELF (Electron localization function) and LOL (Localized orbital locator). The charge transfer within the molecule was identified and frontier molecular orbitals were plotted. The local reactivity descriptors like the local softness and Fukui function were obtained. Molecular docking studies were performed to identify the antiviral activity of the title compound on a couple of viral protein.

2. Procedure

2.1. Experimental details

Ribavirin was purchased from Sigma Aldrich Company with 99% purity and was used as such without any further purification. The FTIR spectrum of the title compound was recorded using a KBr pellet technique in the region 4000–400 cm^{-1} in the evacuation mode with 1.0 cm^{-1} resolution on a PERKIN ELMER FTIR spectrophotometer. The FT Raman spectrum of the title molecule was recorded in the region 4000–100 cm^{-1} in a pure mode using Nd:YAG Laser of 100 mW with 2 cm^{-1} resolution on a BRUCKER RFS 27 at IIT SAIF, Chennai, India.

2.2. Computational method

Becke3-Lee-Yang-Parr (B3LYP) [24] level with 6–311++G(d,p) basis set using Gaussian 09 W [25] program package was employed for all the theoretical computations. Using the Gaussian 09 W software the spectroscopic profiling of the title molecule was carried out in its optimised state. VEDA [26] program enabled percentage potential energy distribution (PED) analysis. In addition, the relative Raman intensities were attained from the scattering activities of the fundamental modes

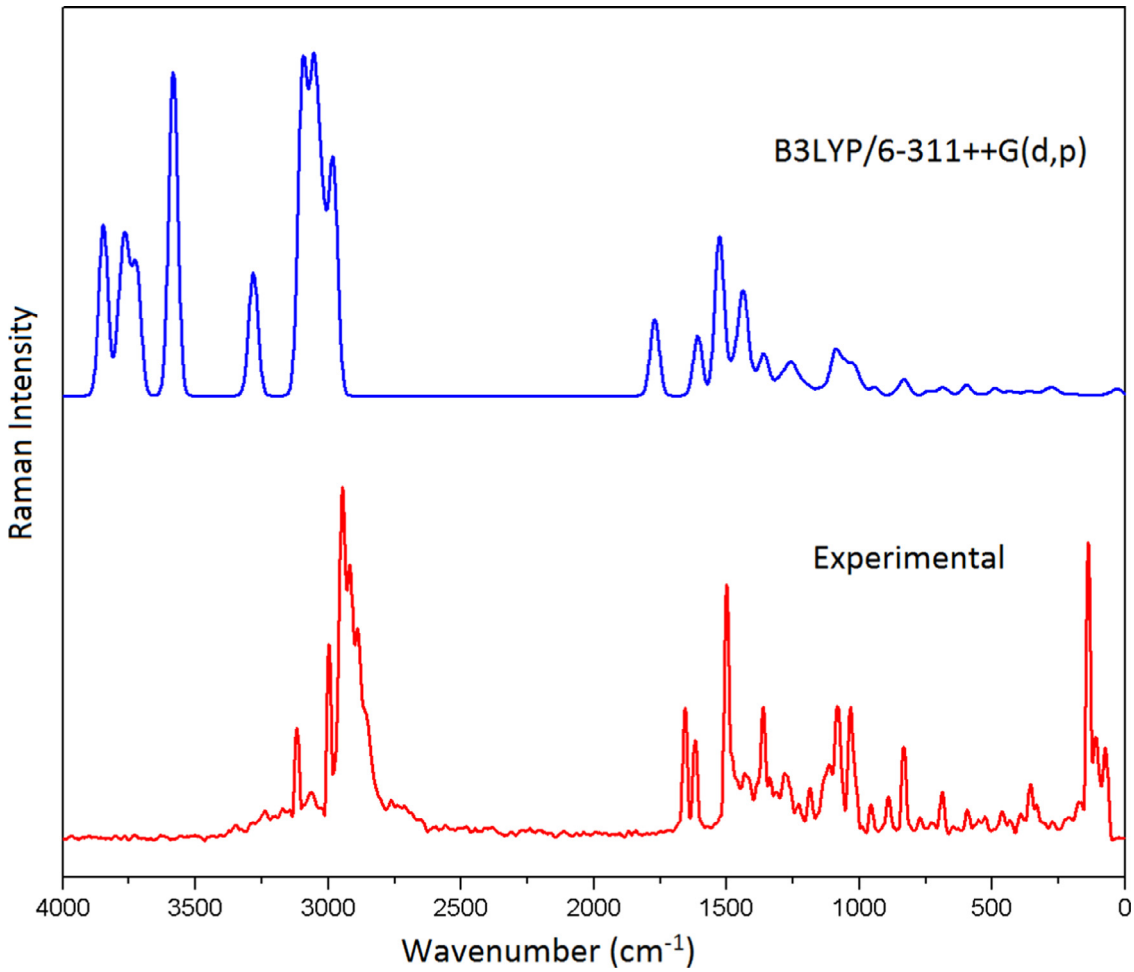

Fig. 2. Comparative FT-Raman spectra of the title compound.

[27,28]. Electrostatic potential (ESP) on molecular vdW (vander Waal) surface is a useful guide to the molecule's reactive behavior, especially in noncovalent interactions [29]. ELF and LOL are tools for performing covalent bonding analysis, as they reveal regions of molecular space where the probability of finding an electron pair is high [30,31]. The Fukui functions are electron density-based local reactivity descriptors, proposed to explain the chemical selectivity or reactivity at a particular site of a chemical system [32]. The analyses such as ESP, Molecular orbitals, Fukui functions, ELF and LOL were finished by Multiwfn 3.4.1 [33], which is a multifunctional wavefunction analysis program. The ESP map was rendered by VMD 1.9.1 program [34] based on the outputs of Multiwfn. Frontier molecular orbitals were plotted and the charge transfer interactions were studied. NBO analysis gives a clear evidence of stabilization originating from hyperconjugation of various intramolecular interactions. The reactive sites of the title compound were identified by calculating the Fukui functions for all the atomic sites. AutoDock Suite 4.2.1 [35] was used to find the minimum binding energy, inhibition constant and various parameters of the ligand-protein docking interactions [36].

3. Data, value and validation

3.1. Molecular geometry

The optimized molecular structure of the title compound with the numbering scheme of the atoms is shown in Fig. 1. The bond parameters such as bond lengths and bond angles obtained from Gaussian software. From the single crystal XRD data [37], it is found that the title compound belongs to the crystal system orthorhombic with P212121 space group and the cell dimensions are as follows; a = 14.863 Å; b = 7.512 Å; c = 8.788 Å. The results are compared with the experimental X-ray diffraction data [33] of the title compound and are listed in Table 1.

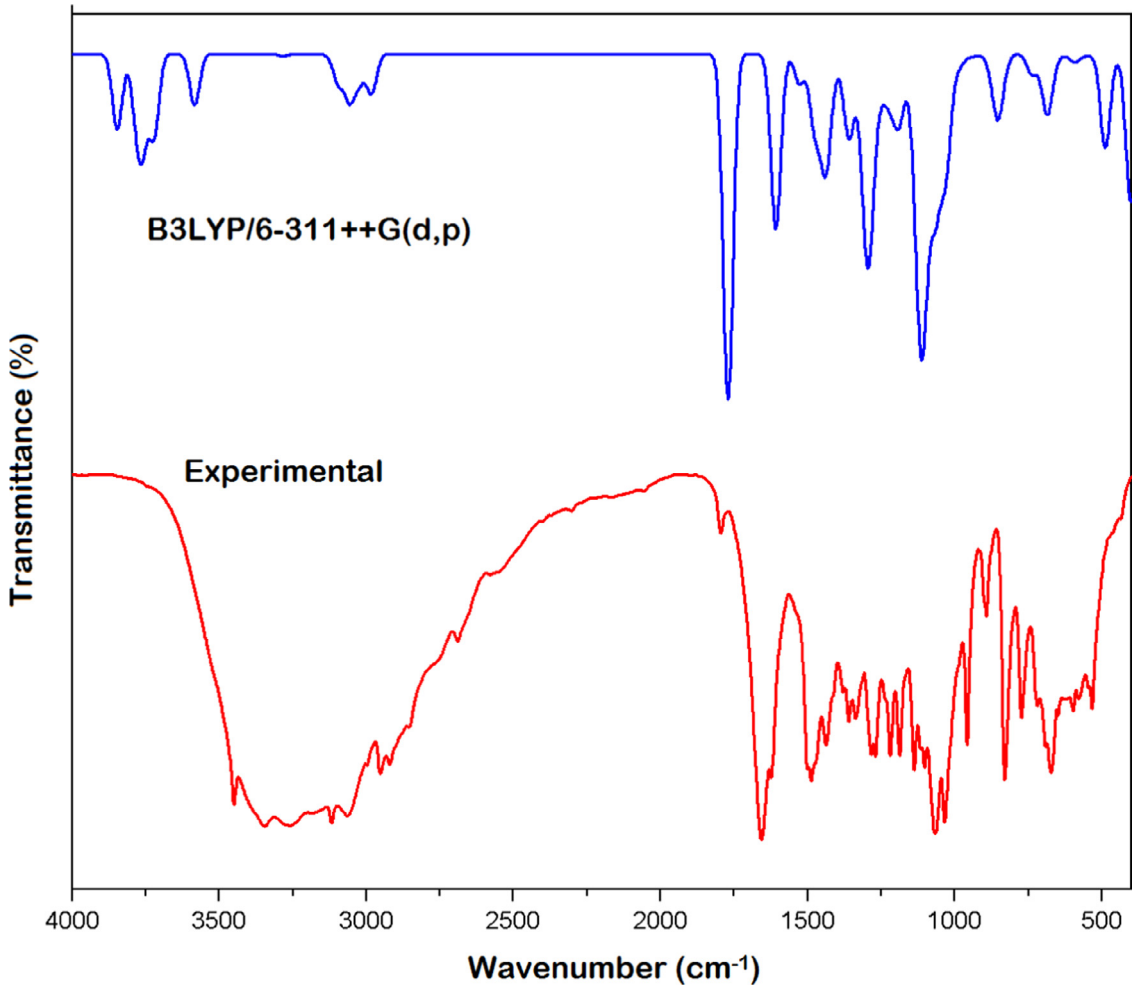

Fig. 3. Comparative FT-IR spectra of the title compound.

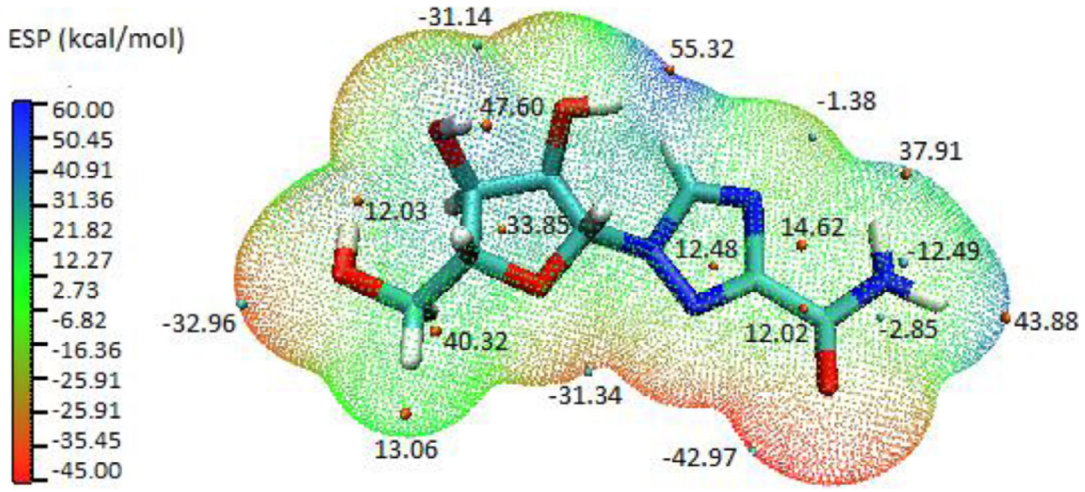

Fig. 4. ESP-mapped molecular vdW surface of the title compound.

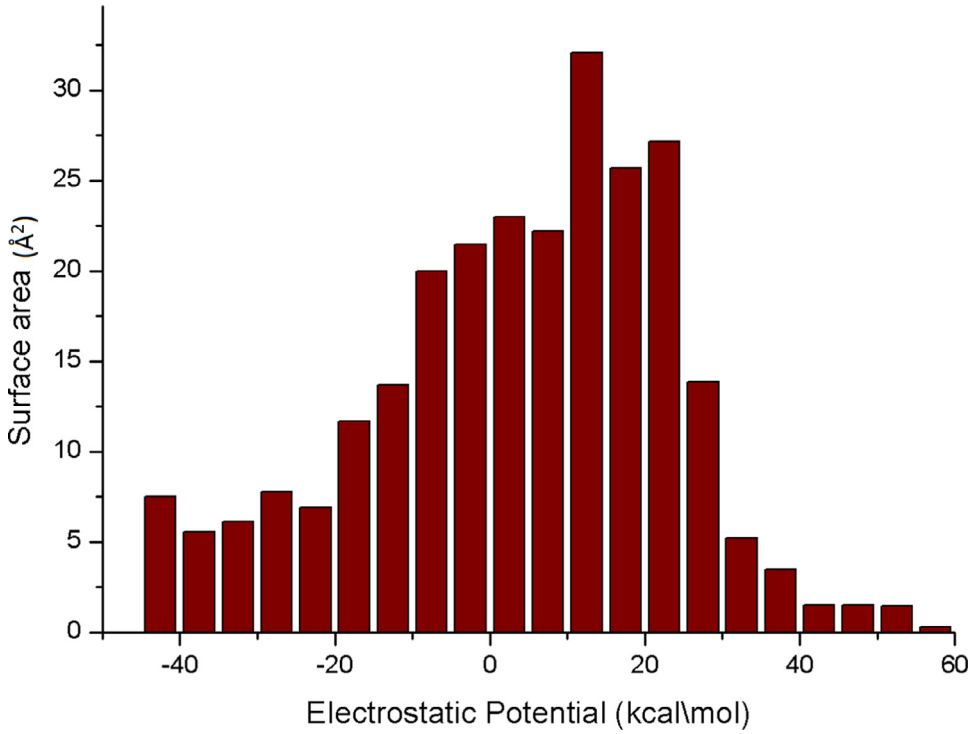

Fig. 5. Surface area in each ESP range on the vdW surface of the title compound.

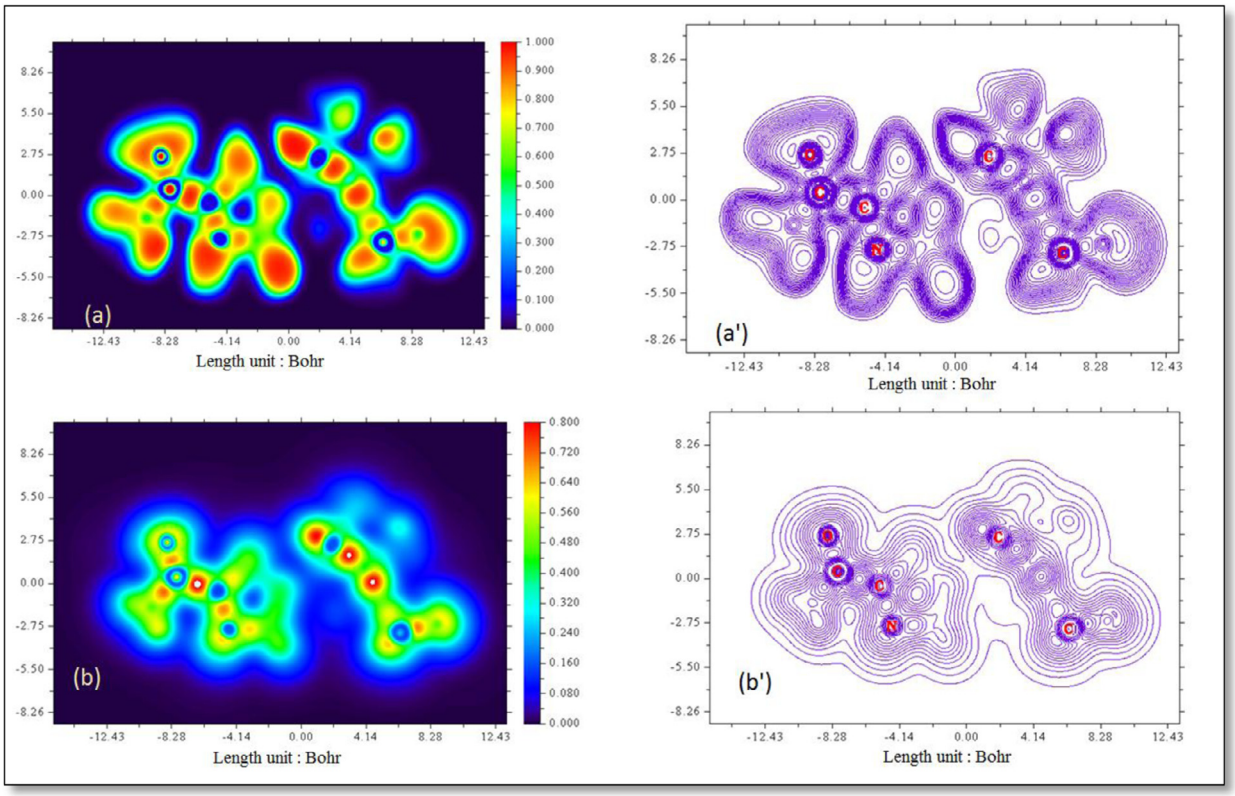

Fig. 6. (a) & (a') ELF, colour filled and contour map of the title compound, (b) & (b') LOL, colour filled and contour map of the title compound.

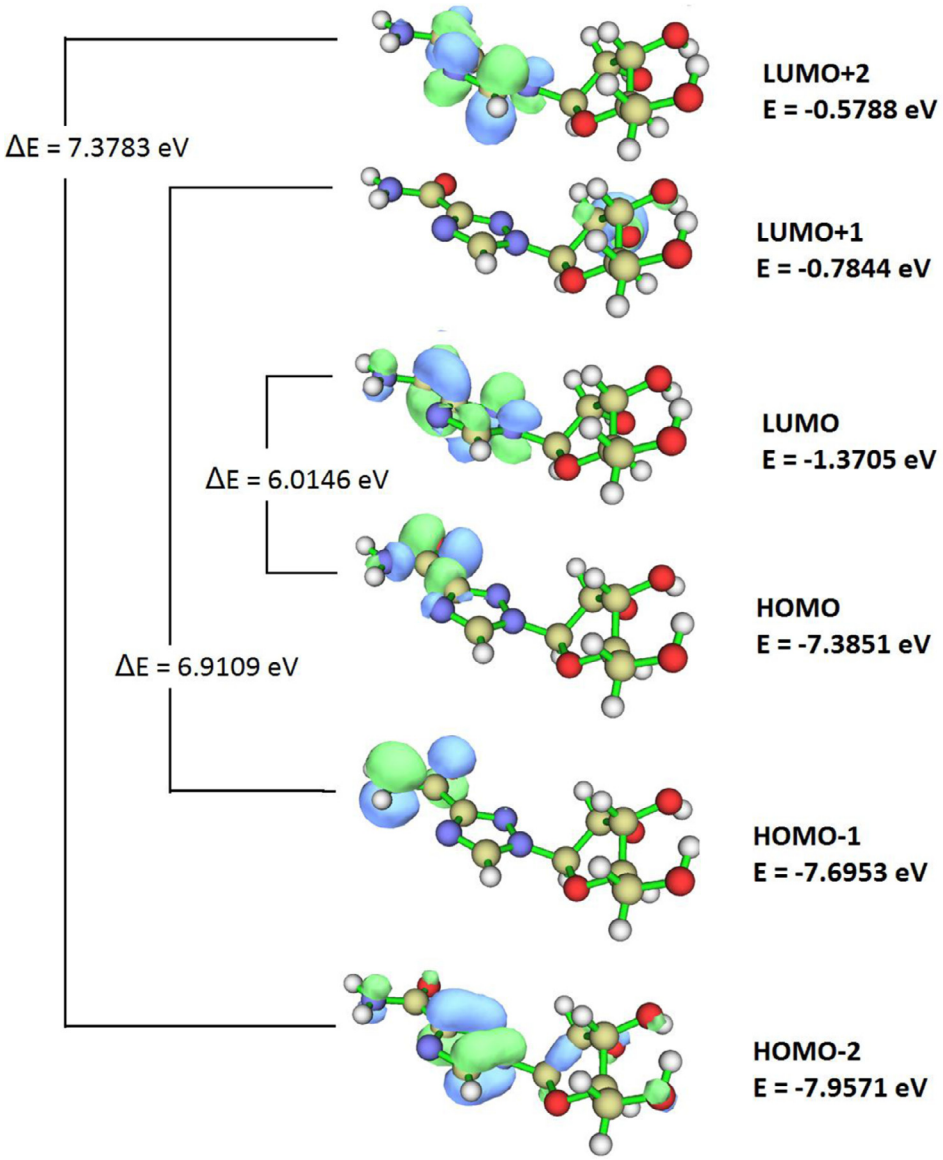

Fig. 7. HOMO – LUMO composition of the title molecule.

3.2. Vibrational assignment

The maximum number of potentially active observable fundamentals of the non-linear molecule is 3N-6, where N is the number of atoms present in the molecule [38]. The title molecule consists of 29 atoms, which has 81 normal modes of vibration. The theoretical and experimental FT-IR and FT-Raman spectra are shown in Figs. 2 and 3 while the spectral assignments along with PED contributions are tabulated in Table 2. The O–H stretching vibrations for organic compounds are expected to arise in the range 3380 ± 200 cm^{-1} [39]. For the title compound, the O–H stretching appears at 3719, 3658 and 3637 cm^{-1} as pure stretching mode as evident from PED value of 100%, 98% and 98% in DFT-B3LYP method and it is in good agreement with the experimental wavenumbers at 3723, 3670, 3630 cm^{-1} and 3720, 3640 cm^{-1} in FT Raman and FT-IR spectrum respectively. The asymmetric and symmetric stretching NH_2 vibrations of the title compound were theoretically calculated at 3599 and 3466 cm^{-1} respectively with a PED 99%. The corresponding wavenumbers were observed at 3460 cm^{-1} in FT-Raman and 3450 cm^{-1} in FT-IR spectrum. The NH_2 bending vibration [40] was observed at 1555 cm^{-1} theoretically and was found to occur at 1560 and 1550 cm^{-1} in FT-Raman and FT-IR spectrum respectively with 82% of PED. The characteristic carbonyl (C=O) stretching vibrations of the IR and Raman spectra occur in the region of 1725 ± 65 cm^{-1} [41]. The C=O stretching vibration for the title compound was found at 1712 cm^{-1} theoretically and can be seen at 1710 and 1720 cm^{-1} in FT-Raman and FT-IR spectrum respectively. An average frequency shift of 700 cm^{-1} is

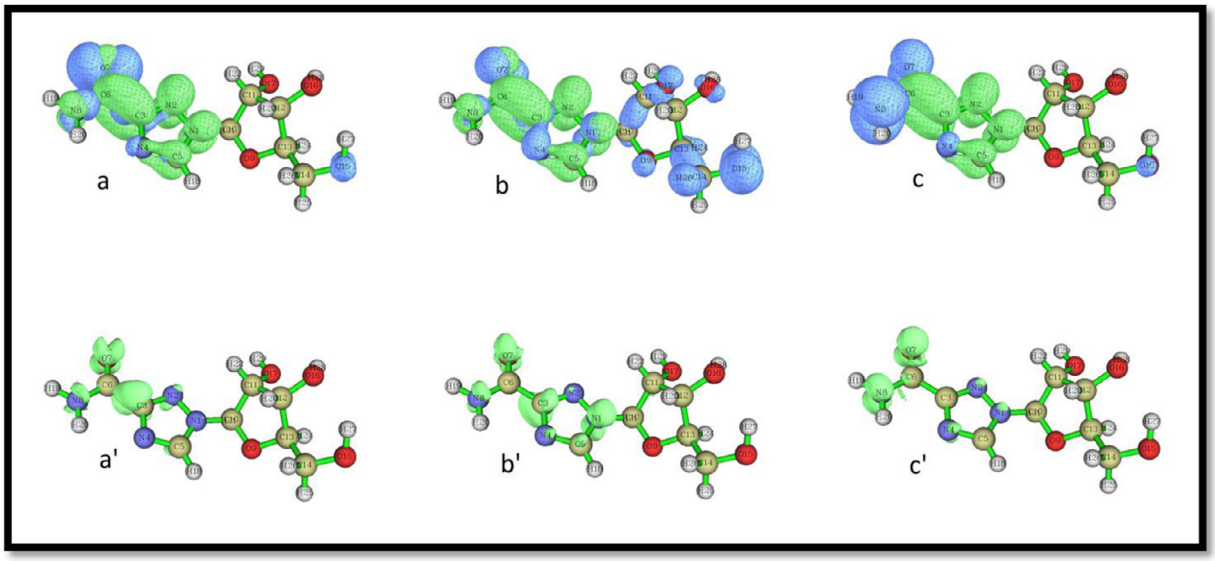

Fig. 8. a), b) & c) Electron – hole distribution for the three excited states of the title compound. a'), b') & c') Electron – hole overlap for the three excited states of the title compound.

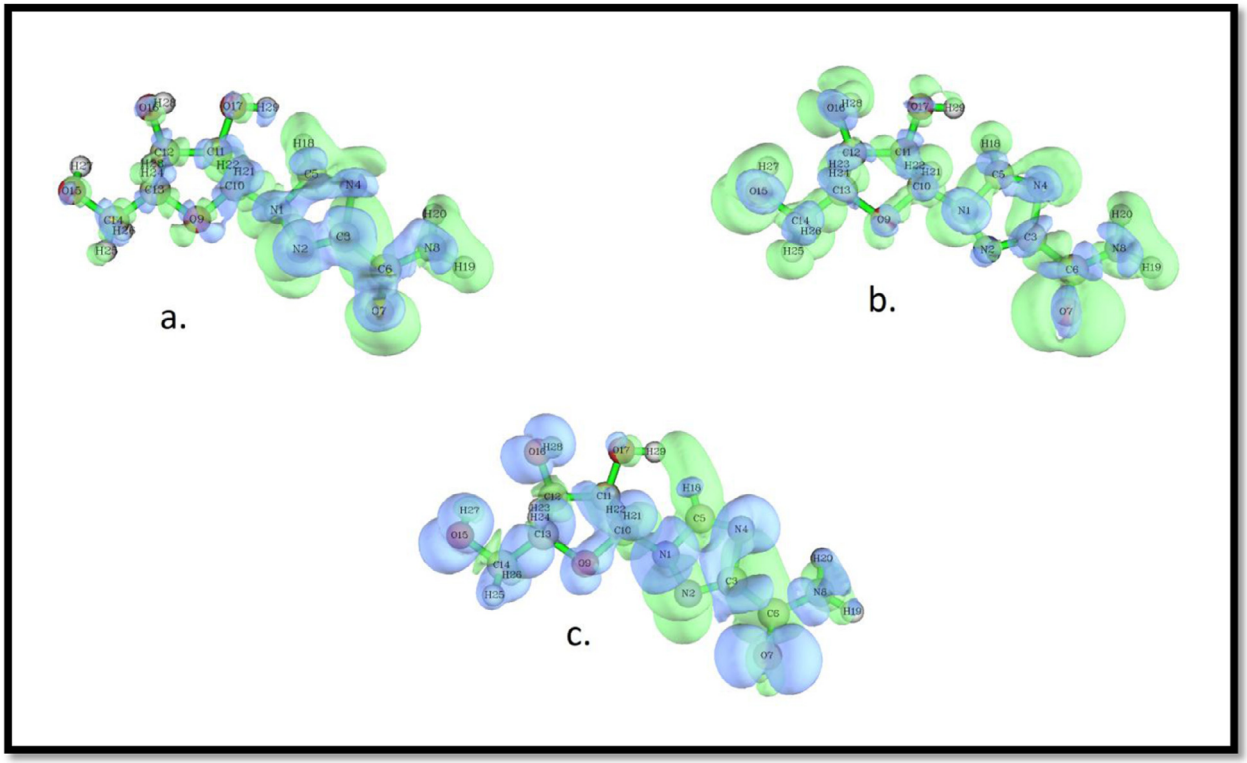

Fig. 9. a) & b) f^{+} & f^{-} Fukui functions of the title compound respectively, c) dual descriptor of the title compound.

observed between the single and double bonded C–O stretching vibrations. The theoretically calculated wavenumbers for C–O stretching vibrations are observed at 1092, 1073, 1036, 1021, 995 cm^{-1}. The corresponding wavenumbers are seen at 1086, 1084, 1005 cm^{-1} in FT-Raman and 1102, 1067, 1034 cm^{-1} in FT-IR spectrum. The C–N stretching is usually seen in the region of 1400–1200 cm^{-1} [42]. Assignment of C–N stretching frequencies is a very difficult task since mixing of bands is possible in this region. For the title compound, the calculated C–N stretching vibrations coupled with other vibrations were

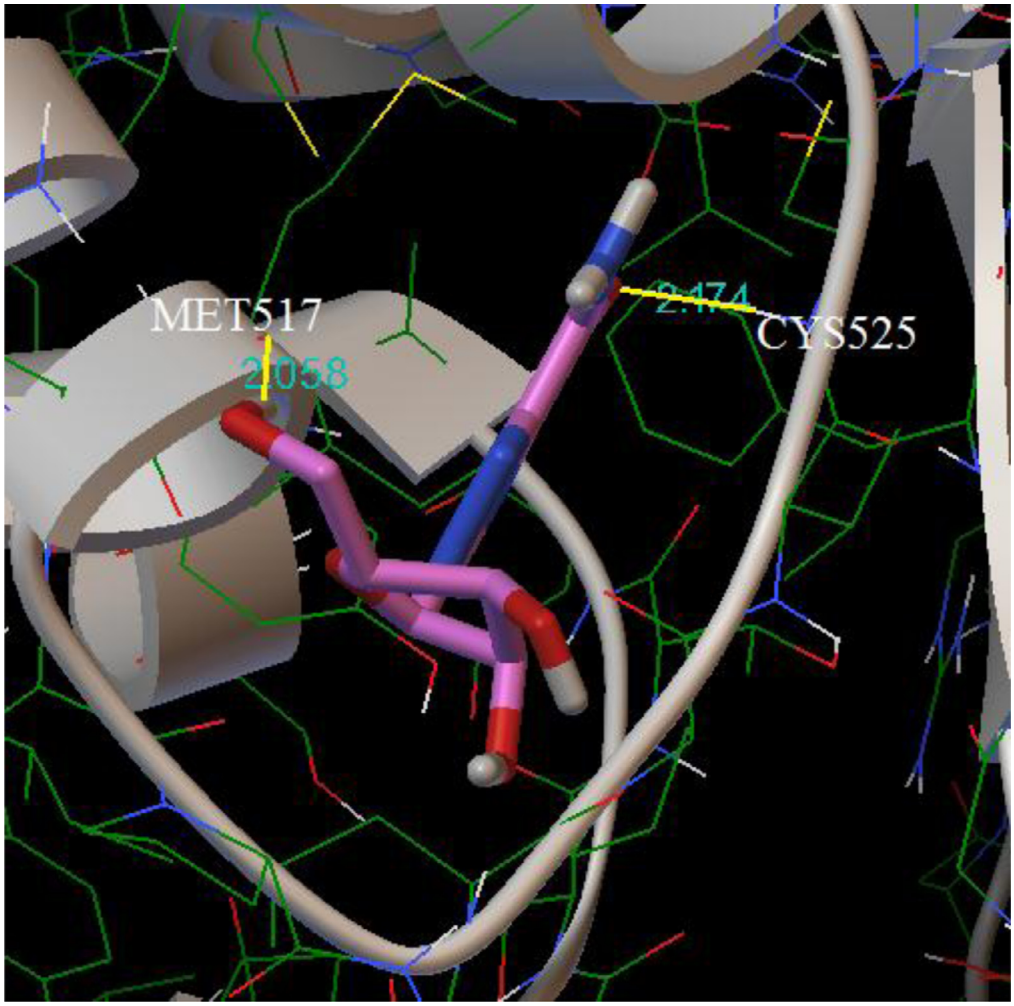

Fig. 10. Docking and hydrogen bond interactions of the title compound with Hepatitis C viral protein.

obtained at 1478, 1390 and 1256 cm^{-1}. The corresponding modes were observed at 1474, 1254 cm^{-1} and 1487, 1269 cm^{-1} in FT-Raman and FT-IR spectrum respectively.

3.3. Topology analyses

The ESP-mapped along with surface extrema of the title compound is shown in Fig. 4 and the graph of surface area plotted against different ESP ranges is shown in Fig. 5. Green and orange spheres represent surface local minima and maxima of ESP respectively. Global minimum on the surface was found to be −42.97 kcal/mol, its large negative value is owing to the lone pair of oxygen O7. The global maximum arising from the positively charged H29, the ESP at this point is much larger (55.32 kcal/mol) than that at other. This is because of the presence of oxygen, which attracted a great deal of electrons from H29. From the Fig. 5, it can be seen that there is a large portion of the molecular surface having small ESP value, namely from −20 to 30 kcal/mol. The regions above and below the triazole ring have an abundant π-electron cloud thus corresponding to the negative part; the positive part mainly arises from the positive charged C–H hydrogens; the near-neutral part represents the border area between the negative and positive parts. There are also small areas having remarkable positive and negative ESP value, corresponding to the regions closed to the global ESP minimum and maximum, respectively.

The topological analyses of the electron localization function (ELF) and the localized orbital locator (LOL) were completed using Multiwfn program. Color shade maps and contour maps of the ELF and LOL for the title molecule are presented in figures. From the Fig. 6, it can be seen that the covalent regions have high LOL value (red regions), the electron depletion regions between valence shell and inner shell are shown by the blue circles around nuclei. A lone pair of oxygen O7 atom is pointed out by purple arrow. A similar picture is seen from the ELF map, the regions around C3, N4, C6 where found to have lesser value where electrons are expected to be delocalized. Whereas the regions around the hydrogen atoms have comparatively large values indicate bonding and nonbonding localized electron. In general, a large ELF or LOL value [31] in a

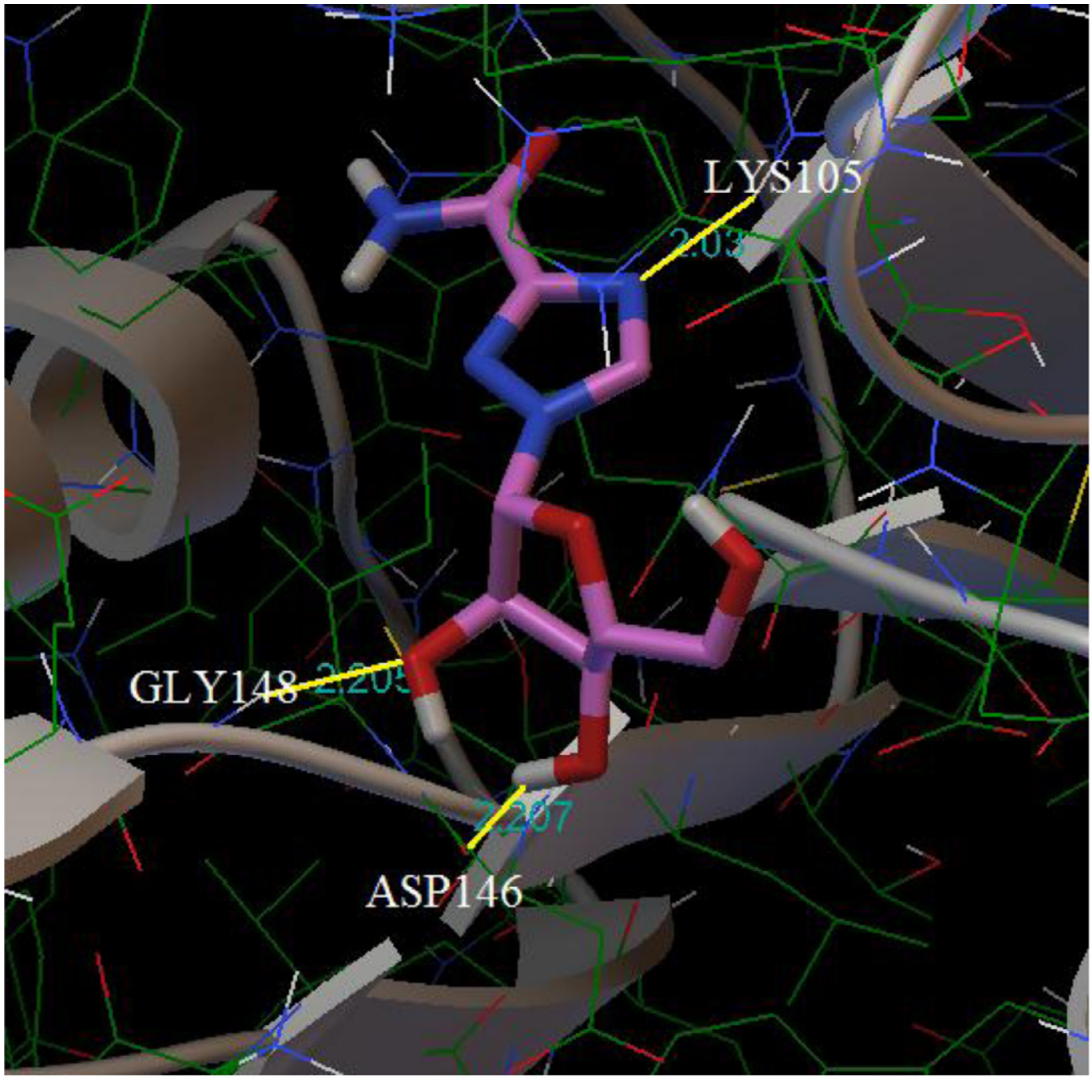

Fig. 11. Docking and hydrogen bond interactions of the title compound with dengue viral protein.

region indicates high localization of electrons, due to the presence of a covalent bond, a lone pair of electrons, or a nuclear shell in that region.

The 3D plots of the HOMOs and LUMOs of the title compound generated using the Multiwfn program from the Gaussian output using B3LYP/6–311++G(d,p) as the basis set are shown in Fig. 7. The band gap energy value of the title molecule calculated from the HOMO-LUMO energies was 6.0146 eV, which confirms that the molecule has a stable structure and the band gap energy value was comparable to the band gap energy value of the bioactive molecules [43,44]. Table 3, presents the HOMO energy, LUMO energy, energy gap, few reactivity descriptors. The HOMO and LUMO values are related to the ionization potential (IP) and electron affinity (EA) of the molecule. The IP value indicates that the energy value of 7.3851 eV is required to remove an electron from the HOMO. The lower value of EA (1.3705 eV) indicates that the title compound readily accepts electrons to form bonds.

To bring out a correlation between the HOMO-LUMO gap and charge transfer, the charge transfer within the molecule due to excitation has been studied. Multiwfn [33] program was used to investigate and visualize the charge transfer due to the excitation. The time dependent DFT (TD-DFT) calculations were made on the title compound using B3LYP/6–311++G(d,p) as the basis set. The diagrams representing the electron-hole (green-blue) distribution and the electron-hole overlap for the 3 excited states are shown in Fig. 8. Table 4 indicates the values of overlap of electron-hole distribution (S), charge transfer length (D), Δr and excitation energy (E) for different excitation modes. The distance between the centroid of hole and electron is a measure of charge transfer length (D); the larger the value, the longer length the charge transfers. Charge-transfer excitation (CT) occurs when the spatial separation of hole and electron is large which lead to movement of charge density from one place to another place. From the table, it can be seen that the charge transfer length of the second excitation

Table 1
Optimized geometrical parameters of the title compound: bond length (Å) and bond angles (°).

Bond length (Å)	Experimental[a]	B3LYP/6–311++G(d,p)	Bond angle (°)	Experimental[a]	B3LYP/6–311++G(d,p)
N1–N2	1.368	1.349	N2–N1–C5	110.5	110.2
N1–C5	1.327	1.354	N2–N1–C10	118.9	119.3
N1–C10	1.475	1.467	N1–N2–C3	101.5	102.7
N2–C3	1.321	1.325	C5–N1–C10	130.8	130.4
C3–N4	1.361	1.365	N1–C5–N4	110.5	109.5
C3–C6	1.487	1.500	N1–C5–H18	–	123.1
N4–C5	1.332	1.319	N1–C10–O9	107.9	107.8
C5–H18	–	1.077	N1–C10–C11	111.4	112.1
C6–O7	1.235	1.217	N1–C10–H21	–	107.7
C6–N8	1.328	1.361	N2–C3–N4	115.5	114.3
N8–H19	–	1.007	N2–C3–C6	122.3	122.5
N8–H20	–	1.008	N4–C3–C6	122.1	123.1
O9–C10	1.393	1.412	C3–N4–C5	102.1	103.3
O9–C13	1.464	1.442	C3–C6–O7	119.4	122.8
C10–C11	1.529	1.550	C3–C6–N8	116.7	112.7
C10–H21	–	1.094	N4–C5–H18	–	127.4
C11–C12	1.523	1.539	O7–C6–N8	123.8	124.5
C11–O17	1.427	1.424	C6–N8–H19	–	118.7
C11–H22	–	1.090	C6–N8–H20	–	120.6
C12–C13	1.519	1.537	H19–N8–H20	–	120.7
C12–O16	1.418	1.409	C10–O9–C13	109.7	109.6
C12–H23	–	1.094	O9–C10–C11	107.7	108
C13–C14	1.509	1.522	O9–C10–H21	–	110.8
C13–H24	–	1.097	O9–C13–C12	104.0	103.3
C14–O15	1.435	1.420	O9–C13–C14	108.3	109.9
C14–H25	–	1.091	O9–C13–H24	–	109.7
C14–H26	–	1.100	C11–C10–H21	–	110.5
O15–H27	–	0.966	C10–C11–C12	101.3	101.9
O16–H28	–	0.968	C10–C11–O17	111.6	111.4
O17–H29	–	0.962	C10–C11–H22	–	111.5
			C12–C11–O17	106	106.7
			C12–C11–H22	–	113.7
			C11–C12–C13	101.6	102.0
			C11–C12–O16	109.7	114.9
			C11–C12–H23	–	109.2
			O17–C11–H22	–	111.3
			C11–O17–H29	–	109.7
			C13–C12–O16	113.6	114.7
			C13–C12–H23	108.3	108.9
			C12–C13–C14	117.7	114.7
			C12–C13–H24	–	109.8
			O16–C12–H23	–	106.9
			C12–O16–H28	–	107.4
			C14–C13–H24	–	109.1
			C13–C14–O15	110.2	110.8
			C13–C14–H25	–	110.0
			C13–C14–H26	–	109.6
			O15–C14–H25	–	106.7
			O15–C14–H26	–	111.6
			C14–O15–H27	–	108.9
			H25–C14–H26	–	108.0

[a]Ref [37].

mode is comparatively larger and Δr is also higher for the same mode indicating the fact that the second excitation mode corresponds to a strong charge transfer excitation. Even though the overlap integral of electron-hole distribution was found to be small in the first excited state, the charge transfer length is comparatively lesser.

3.4. Fukui functions and reactive sites

The key concepts in selectivity are the Fukui function and the local softness; a highly electrophilic/nucleophilic center is a site presenting a high value of the associated Fukui function. New descriptors such as dual descriptor (Δf(r)), a condensed version of Δf(r) (Δs_k) were also calculated for better understanding [45]. Dual descriptor (Δf(r)) [45], is given by: $\Delta f(r) = f^{+}(r)\text{-}f^{-}(r)$. If Δf(r) > 0, then the site is favored for a nucleophilic attack, whereas if Δf(r) < 0, then the site could hardly be susceptible to undertake a nucleophilic attack but it may be favored for an electrophilic attack. Δs_k a condensed version [46] of Δf(r) multiplied by the molecular softness (S) is given by: $\Delta s_k = S\,(f_k^{+}\text{-}f_k^{-}) = (s_k^{+}\text{-}s_k^{-})$. The interpretation is similar to Δf(r). Table 5, presents the mulliken atomic charge, Fukui functions, local softness values of all the atoms of the

Table 2
Calculated vibrational frequencies (cm^{-1}) assignments of the title compound based on B3LYP/6–311++G(d,p) basis set.

Mode no	Experimental wave number (cm^{-1})		Theoretical wave numbers (cm^{-1})		I_{IR}[b]	I_{RAMAN}[c]	Assignments (PED%)[d]
	FT-Raman	FT-IR	Unscaled	Scaled[a]			
81	3723	3720	3846	3719	22	53	ϒ OH (100)
80	3670	–	3782	3658	15	23	ϒ OH (98)
79	3630	3640	3761	3637	23	37	ϒ OH (98)
78	–	–	3722	3599	23	38	Υ_{as} NH_2 (99)
77	3460	3450	3584	3466	15	100	Υ_{ss} NH_2 (99)
76	–	–	3282	3173	1	38	ϒ CH (99)
75	2999	2997	3102	3000	3	37	ϒ CH (99)
74	2993	2992	3093	2991	6	65	Υ_{as} CH_2 (95)
73	2957	–	3058	2957	11	7	ϒ CH (94)
72	2949	2953	3055	2955	2	84	ϒ CH (97)
71	2922	2920	3024	2924	8	51	ϒ CH (91)
70	2880	2890	2982	2884	11	71	Υ_{ss} CH_2 (94)
69	1710	1720	1771	1712	100	23	ϒ C=O (73)
68	1560	1550	1608	1555	51	18	β NH_2 (82)
67	1474	1487	1528	1478	8	46	ϒ NC (67)
66	–	1469	1515	1465	1	4	β CH_2 (90)
65	–	–	1476	1428	21	8	β HCN (12) + ϒ CC (59)
64	–	–	1444	1396	15	12	β HCO (47)
63	–	–	1438	1390	6	8	β HCO (27) + ϒ NC (15)
62	1387	–	1435	1388	10	10	β HCO (17)
61	–	1379	1425	1378	4	2	β HCO (76)
60	1366	1361	1407	1361	2	4	β HCC (63)
59	1337	1336	1381	1335	2	3	β HCO (63)
58	–	–	1362	1317	15	4	ϒ CC (45) + β HCO (19)
57	–	–	1355	1311	9	7	ϒ CC (19) + β HCO (40)
56	–	1284	1331	1287	1	1	β HCN (32)
55	–	–	1319	1275	1	0	β HCO (57)
54	–	–	1318	1274	7	1	TORS HCOH (59)
53	1254	1269	1299	1256	36	3	ϒ NC (35)
52	–	–	1287	1245	24	2	β HOC (50)
51	–	1219	1267	1226	6	5	β HCC (43)
50	–	–	1248	1207	6	6	β HCO (21) + ϒ NC (19)
49	1192	1187	1222	1182	11	3	β HOC (69)
48	–	–	1196	1156	13	2	β HCN (58)
47	–	1138	1180	1141	9	1	β HOC (64)
46	1120	1110	1150	1112	3	2	ϒ CC (53)
45	1086	1102	1130	1092	28	1	ϒ OC (58) + ϒ CC (12)
44	1084	1067	1110	1073	67	0	ϒ OC (59)
43	–	–	1095	1059	4	9	β HNC (52) + ϒ NC (13)
42	–	–	1088	1052	2	3	ϒ CC (18)
41	–	1034	1072	1036	32	4	ϒ OC (75)
40	–	–	1056	1021	14	3	ϒ OC (46)
39	–	–	1048	1014	3	4	ϒ NN (45)
38	1005	–	1029	995	29	2	ϒ OC (48)
37	–	982	1017	984	1	7	β CNC (36) + ϒ NC (28)
36	–	958	986	953	4	2	ϒ CC (52)
35	897	892	942	911	1	3	ϒ CC (16) + τ HCOH (20)
34	–	–	876	847	3	0	τ HCNN (86)
33	818	829	853	825	17	1	ϒ CH (10) + ϒ NC (27)
32	–	–	830	803	2	4	β HCO (25) + τ HCOH (17)
31	–	773	817	790	0	1	τ NCCO (81)
30	704	720	737	713	6	1	τ CCCN (30)
29	675	672	692	669	3	1	ϒ NC (10) + β CCO (25) + τ NCCO (13)
28	–	–	689	666	8	1	τ NCCO (55)
27	–	648	678	656	7	1	β COC (45)
26	620	–	647	625	1	0	τ CNNC (71)
25	–	578	597	577	1	3	β CCC (24) + ϒ CC (10)
24	561	–	587	568	1	0	τ HNCC (87)
23	–	534	546	528	0	0	β CNN (44)
22	–	–	489	473	1	2	β CCO (36)
21	471	–	488	472	26	1	τ HOCC (60) + τ CCCO (16)
20	430	–	438	423	1	1	ϒ CC (10) + β NCO (38)
19	–	–	403	390	20	0	β CNN (10) + β CCC (16)
18	–	–	401	388	23	0	β CCC (32)
17	361	–	363	351	1	1	β CCO (43) + β CCO (20)

(*continued on next page*)

Table 2 (*continued*)

Mode no	Experimental wave number (cm^{-1})		Theoretical wave numbers (cm^{-1})		I_{IR}[b]	I_{RAMAN}[c]	Assignments (PED%)[d]
	FT-Raman	FT-IR	Unscaled	Scaled[a]			
16	–	–	356	344	2	1	τ COCC (30) + β CCO (14)
15	318	–	313	303	20	1	β CCO (10) + τ NCCN (12)
14	–	–	306	296	34	0	τ HNCO (56)
13	–	–	283	274	23	1	τ HCOH (44) + τ HCOH (36)
12	–	–	275	266	1	2	τ HCOH (14) + τ HCOH (17) + τ HCNC (15)
11	–	–	258	249	7	0	τ HCOH (11) + τ CCCO (34) + τ HCOH (11)
10	234	–	246	238	1	1	τ HCOC (16) + τ HCCH (13) + τ HCOH (13)
9	–	–	194	187	2	0	τ COCC (20)
8	181	–	191	185	1	0	τ HNCC (14) + τ NCCN (12)
7	118	–	124	120	1	0	BEND CCO (10)
6	–	–	111	108	2	0	τ HCCH (22) + τ HNCC (10) + τ HCOH (26)
5	–	–	94	91	1	0	τ HNCC (10) + τ CNCO (40)
4	–	–	72	70	0	0	τ NCCN (30) + τ NCCN (15)
3	54	–	53	51	0	1	τ NCCN (43)
2	–	–	29	28	1	1	τ CNCO (57)
1	–	–	19	18	1	1	τ HCOC (51)

[a] Scaling factor: 0.961 for B3LYP/6–311++G(d,p).
[b] Relative absorption intensities normalized with highest peak absorption equal to 100.
[c] Relative Raman intensities normalized to 100.
[d] Υ-stretching, Υ_s -Symmetrical stretching, Υ_{as} -asymmetrical stretching, β -bending, τ -torsion,

Table 3
Calculated energy values of the title compound by B3LYP/6- 311++G(d,p) method.

Parameters	Values
E_{HOMO} (eV)	−7.3851
E_{LUMO} (eV)	−1.3705
Ionisation Energy	7.3851
Electron Affinity	1.3705
Energy gap (eV)	6.0146
Electronegativity (χ)	4.3778
Chemical potential (μ)	−4.3778
Chemical hardness (η)	3.0073
Chemical softness (s)	0.1663
Electrophilicity index (ω)	3.1864

Table 4
Overlap integral, charge transfer length, Δr and excitation energy for different excited states.

Excitation states	Overlap integral of electron-hole (S)	Charge transfer length (D) Å	Δr (Å)	Excitation energy (E) eV
1	0.1890	1.5164	2.3157	4.4119
2	0.2639	2.7204	3.2156	5.2224
3	0.2343	1.7945	2.2801	5.3071

title molecule. Fig. 9 gives a pictorial representation of fukui functions and dual descriptors, where blue regions correspond to negative regions prone to electrophilic attack and the green regions are positive areas prone to nucleophilic attack. From the table and the figure, it is evident that most of the atomic sites in the molecule are ready to undergo electrophilic attack rather than nucleophilic attack. Δf(r) value is negative for all the nitrogen and oxygen atoms indicating their favor for an electrophilic attack. All the carbon atoms except C11 and C13 are favorable for a nucleophilic attack.

3.5. Molecular docking studies

The antiviral activity of the title compound docked into the active sites of the target proteins was studied from docking parameters. A Dengue RNA viral protein 1R6A [47] and a Hepatitis C viral protein 1HEI [48] were chosen to study the antiviral property of the ligand. The pdb structures of the target proteins are downloaded from RCSB (Research Collaboratory for Structural Bioinformatics) protein data bank (http://www.rcsb.org/pdb/home/home.do). Docked conformation which had the lowest binding energy was chosen to study the mode of binding. The molecular docking binding energies (kcal/mol)

Table 5
Mulliken charge distribution, Fukui function and local softness of the title compound.

Atoms	Mulliken atomic charges			Fukui functions			Local softness		
	N	N-1	N+1	f+	f-	Δf	s+	s-	Δs
1 N	0.1950	−0.3317	0.1821	−0.0129	0.5268	−0.5396	−0.0023	0.0922	−0.0944
2 N	0.0452	−0.1942	−0.1563	−0.2015	0.2394	−0.4409	−0.0353	0.0419	−0.0772
3 C	−0.2366	0.3567	−0.2482	−0.0116	−0.5933	0.5816	−0.0020	−0.1038	0.1018
4 N	−0.1158	−0.4453	−0.1938	−0.0781	0.3295	−0.4076	−0.0137	0.0577	−0.0713
5 C	0.1531	0.3167	0.0525	−0.1005	−0.1636	0.0631	−0.0176	−0.0286	0.0110
6 C	0.1493	0.6130	0.1825	0.0332	−0.4638	0.4970	0.0058	−0.0812	0.0870
7 O	0.0533	−0.3389	−0.4126	−0.4659	0.3921	−0.8580	−0.0815	0.0686	−0.1502
8 N	0.0594	−0.5840	−0.4343	−0.4937	0.6435	−1.1372	−0.0864	0.1126	−0.1990
9 O	0.0656	−0.4891	−0.0362	−0.1018	0.5547	−0.6565	−0.0178	0.0971	−0.1149
10 C	0.0718	0.3434	−0.3408	−0.4125	−0.2717	−0.1409	−0.0722	−0.0475	−0.0246
11 C	0.0779	0.0981	−0.0583	−0.1362	−0.0202	−0.1160	−0.0238	−0.0035	−0.0203
12 C	0.0841	0.0722	−0.3635	−0.4476	0.0119	−0.4595	−0.0783	0.0021	−0.0804
13 C	0.0902	0.1771	−0.0622	−0.1524	−0.0868	−0.0656	−0.0267	−0.0152	−0.0115
14 C	0.0964	0.0001	0.0844	−0.0120	0.0963	−0.1084	−0.0021	0.0169	−0.0190
15 O	0.1026	−0.4259	−0.2273	−0.3299	0.5285	−0.8584	−0.0577	0.0925	−0.1502
16 O	0.1087	−0.4268	−0.1179	−0.2266	0.5355	−0.7621	−0.0397	0.0937	−0.1334
17 O	0.1149	−0.5189	−0.1506	−0.2655	0.6337	−0.8992	−0.0465	0.1109	−0.1574
18 H	0.1210	0.1920	−0.0761	−0.1971	−0.0710	−0.1261	−0.0345	−0.0124	−0.0221
19 H	0.1272	0.3310	0.2868	0.1596	−0.2038	0.3634	0.0279	−0.0357	0.0636
20 H	0.1334	0.3327	0.2527	0.1194	−0.1993	0.3187	0.0209	−0.0349	0.0558
21 H	0.1395	0.1415	0.0962	−0.0433	−0.0020	−0.0413	−0.0076	−0.0003	−0.0072
22 H	0.1457	0.1565	0.1197	−0.0260	−0.0108	−0.0152	−0.0045	−0.0019	−0.0027
23 H	0.1519	0.1610	−0.3674	−0.5192	−0.0092	−0.5101	−0.0909	−0.0016	−0.0893
24 H	0.1580	0.1320	0.1178	−0.0402	0.0260	−0.0662	−0.0070	0.0046	−0.0116
25 H	0.1642	0.1812	0.1773	0.0131	−0.0170	0.0301	0.0023	−0.0030	0.0053
26 H	0.1703	0.1495	0.1009	−0.0694	0.0209	−0.0903	−0.0121	0.0037	−0.0158
27 H	0.1765	0.3437	0.1969	0.0204	−0.1672	0.1877	0.0036	−0.0293	0.0328
28 H	0.1827	0.3393	0.2569	0.0742	−0.1567	0.2309	0.0130	−0.0274	0.0404
29 H	0.1888	0.3170	0.1386	−0.0502	−0.1282	0.0780	−0.0088	−0.0224	0.0137

Table 6
Docking parameters of the title compound docked into the active sites of the target protiens.

Protein (PDB ID)	Bonded residues	Hydrogen bond interactions (ligand…protein)	Bond distance (Å)	Estimated inhibition constant (mM)	Binding energy (kcal/mol)	Intermolecular energy (kcal/mol)	Reference RMSD (Å)
1R6A (Dengue)	GLY148	O….HN	2.205	15.94	−2.90	−4.69	47.81
	LYS105	N….HN	2.030				
	ASP146	OH….O	2.207				
1HEI (HCV)	MET517	OH….O	2.058	2.59	−3.53	−3.02	46.78
	CYS525	O….HN	2.174				

and inhibition constants (mM) were also obtained and listed in Table 6. The interactions of title compound taken as the ligand with both the viral proteins are shown in Figs. 10 and 11. Among them, Hepatitis C viral protein exhibits the lowest binding energy at −3.53 kcal/mol with two hydrogen bonds involving OH..O and O..HN with RMSD value of 46.78 Å. It can be seen that the H27 and O7 from the ligand are involved in the hydrogen bond formation. From the ESP map (Fig. 4) the global minimum values were found at O7 indicating the electrophilic nature of the oxygen atom. From fukui function result (Table 5) H27 was found to have the lowest value of Δs_k (−0.00012), which indicates that this hydrogen atom acts as a nucleophile while binding to the target protein. Thus the topological analyses of the molecular structure complement the results obtained from the molecular docking studies. Docking results from previous studies [49] shows that the energy value obtained from the docking of Ribavirin with receptor Angiotensin converting enzyme 2 was zero, indicating very low binding affinity towards SARS (Severe Acute Respiratory Syndrome). The antiviral action of ribavirin discussed above showed a better affinity towards viral proteins including dengue virus. Knowledge of Protein-Ligand interaction helps in designing new anti-viral drugs in the future.

4. Conclusion

In the present work, the experimental and theoretical spectroscopic and topological analyses of Ribavirin using FT-IR, FT-Raman and tools derived from the DFT has been reported. In general, a good agreement within experimental and theoretical normal modes of vibrations was found. Employing the DFT/B3LYP method with 6–311++G(d,p) basis set, the optimized molecular geometry, vibrational frequencies along with infrared intensities and Raman activity of the molecule have been

calculated. Frontier Molecular Orbitals analysis reveals the presence of ICT within the molecule, which is further confirmed by the charge transfer interactions due to excitation. The HOMO and LUMO energy values were calculated from which the band gap energy of the title compound was determined to be 6.0146 eV. The electron distribution and the reactive sites on the surface of the title compound were analysed using ESP, ELF and LOL. Fukui functions, local softness for all the atomic sites of the molecule were calculated. In addition, the molecular docking output shows that the title compound acts as a good antiviral agent against the Hepatitis C viral protein, with a low binding energy of −3.53 kcal/mol.

References

[1] H. Saad, Synthesis of some pyridyloxymethyl-oxadiazoles, thiadiazoles and triazoles of expected pharmacological activity, Indian J. Chem. 35B (1996) 980–984.
[2] I.B. Obot, N.O. Obi-Egbedi, S.A. Umoren, E.E. Ebenso, Adsorption and kinetic studies on the inhibition potential of fluconazole for the corrosion of Al in HCl solution, Chem. Eng. Comm. 198 (2011) 711–725.
[3] I.B. Obot, N.O. Obi-Egbedi, Adsorption properties and inhibition of mild steel corrosion in sulphuric acid solution by ketoconazole experimental and theoretical method, Corros. Sci. 52 (2010) 198–204.
[4] M.M. Antonijevic, S.M. Milic, M.B. Petrovic, Films formed on copper surface in chloride media in the presence of azoles, Corros. Sci. 51 (2009) 1228–1237.
[5] L. Wang, Inhibition of mild steel corrosion in phosphoric acid solution by triazole derivatives, Corros. Sci. 48 (2006) 608–616.
[6] I.B. Obot, A.S. Johnson, Ab initio, DFT and TD-DFT electronic absorption spectra investigations on 3,5-diamino-1,2,4-triazole, Elixir Comp. Chem. 43 (2012) 6658–6661.
[7] V. Krishnakumar, R. John Xavier, FT Raman and FT–IR spectral studies of 3-mercapto-1,2,4-triazole, Spectrochimica Acta Part A 60 (2004) 709–714.
[8] D. Cecily Mary Glory, R. Madivanane, K. Sambathkumar, Electronic Structure Investigations of 3 and 5- Diamino-1,2,4-Triazole By UV–Visible, NMR spectral studies and homo-lumo analysis by AB Initio and DFT calculations, Elixir Comp. Chem. 89 (2015) 36730–36741.
[9] R.W. Sidwell, J.H. Huffman, G.P. Khare, L.B. Allen, J.T. Witkowski, R.K. Robins, Broad-spectrum antiviral activity of Virazole: 1-f8- D-Ribofuranosyl-1,2,4-triazole- 3-carboxamide, Science 177 (1972) 705–706.
[10] J.T. Witkowski, R.K. Robins, R.W. Sidwell, L.N. Simon, Design, synthesis, and broad spectrum antiviral activity of 1-.beta.-D-ribofuranosyl-1,2,4-triazole-3-carboxamide and related nucleosides, J. Med. Chem. 15 (1972) 1150–1154.
[11] M. Tisdale, D.J. Bauer, The relative potencies of anti-influenza compounds, Ann. N.Y. Acad. Sci. 284 (1977) 254.
[12] E.L. Stephen, J.W. Dominik, J.B. Moe, J.S. Walker, Therapeutic effects of ribavirin given by the intraperitoneal or aerosol route against influenza virus infections in mice, Antimicrob. Agents Chemother. 10 (1976) 549–554.
[13] E.W. Larson, E.L. Stephen, J.S. Walker, Therapeutic effects of small-particle aerosols of ribavirin on parainfluenza (Sendai) virus infections of mice, Antimicrob. Agents Chemother 10 (1976) 770–772.
[14] J.N. Dowling, B. Postic, L.O. Guevarra, Effect of ribavirin on murine cytomegalovirus infection, Antimicrob. Agents Chemother. 10 (1976) 809–813.
[15] E. Declercq, M. Luczak, D. Shugar, P.F. Torrence, J.A. Waters, B. Witkop, Effect of cytosine arabinoside, lododeoxyuridine, ethyldeoxyuridine, thiocyanatodeoxyuridine, and ribavirin on tail lesion formation in mice infected with vaccinia virus, Proc. Sac. Exp. Biol. Med. 151 (1976) 487–490.
[16] J.B. Arensman, J.W. Dominik, D.E. Hilmas, Effects of small-particle aerosols of rimantadine and ribavirin on arterial blood pH and gas tensions and lung water content of A2 influenza-infected mice, Antimicrob. Agents Chemother. 12 (1977) 40–46.
[17] C.B. Zuniga, C. Almeida, A.C.L. Iervoline, I.O . Castro, P.A.A. Galvao, Action of 1-beta-D ribofuranosyl-1, 2, 4,-triazole-3-carboxamide (viramid, ICN 1229) in the treatment of acute viral hepatitis, Rev. Assoc. Med. Bras. 20 (1974) 386–390.
[18] P.A.A. Galvao, I. 0. Castro, Treatment of acute viral hepatitis with a new antiviral compound, Rev. Bras. Clin. Ter. 3 (1975) 221–228.
[19] P.A.A. Galvao, I. 0. Castro, The effect of l-β-d-ribofuranosyl208;1,2,4-triazole-3-carboxamide on acute viral hepatitis, Ann. A'. Y. Acad. Sci. 284 (1977) 278–283.
[20] D. Huggins, G.J.M. Pereira, The use of virazole as a therapeutic aid in viral acute hepatitis, Rec. Bras. Med. 34 (1977) 307–320.
[21] L.B. Allen, K.H. Boswell, T.A. Khwaja, R.B. Meyer Jr., R.W. Sidwell, J.T. Witkowski, Synthesis and antiviral activity of some phosphates of the broad-spectrum antiviral nucleoside, l-β-D-Ribofuranosyl-1,2,4-triazole-3-carboxamide (Ribavirin), J. Med. Chem. 21 (8) (1978) 742–746.
[22] L. Dudycz, D. Shugar, E. De Clercq, J. Descamps, Synthesis and determination of antiviral activity of the 2'(3')-O-Methyl derivatives of Ribavirin (l-β-D-Ribofuranosyl-1,2,4-triazole-3-carboxamide), J. Med. Chem. 20 (10) (1977) 1354–1356.
[23] R.D. Zakharieva, A.S. Galabovb, N. Nikolovab, Synthesis and antiviral activity of amino acid esters of ribavirin, Bioorganic Med. Chem. Lett. 4 (24) (1994) 2831–2832.
[24] A.D. Becke, Density-functional thermochemistry. III. The role of exact exchange, J. Chem. Phys. 98 (1993) 5648–5652.
[25] M.J. Frisch, G.W. Trucks, H.B. Schlegel, G.E. Scuseria, M.A. Robb, J.R. Cheeseman, G. Scalmani, V. Barone, B. Mennucci, G.A. Petersson, H. Nakatsuji, M. Caricato, X. Li, H.P. Hratchian, A.F. Izmaylov, J. Bloino, G. Zheng, J.L. Sonnenberg, H.M. Ehara, M. Toyota, K. Vreven, T. Montgomery, J.A. Perlta, J.E. Ogliaro, F. Bearpark, M. Heyd, J.J. Brothers, E. Kudin, K.N. Staroverov, V.N. Kobayashi, R. Normand, J. Raghavachari, K. Rendell, A. Burant, J.C. Iyengar, S.S. Tomasi, J. Cossi, M. Rega, N. Millam, J.M. Klene, M. Knox, J.E. Cross, J.B. Bakken, V. Adamo, C. Jaramillo, J. Gomperts, R. Stratmann, R.E. Yazyev, O. Austin, A.J. Cammi, R. Pomelli, C. Ochterski, J.W. Martin, R.J. Morokuma, K. Zakrzewski, V.G. Voth, G.A. Salvador, P. Dannenberg, J.J. Dapprich, S. Daniels, A.D. Farkas, O. Foresman, J.B. Ortiz, J.V. Ciolslowski, J. Fox, D.J. Gaussian 09, Revision E.01, Gaussian, Inc, Wallingford CT, 2009.
[26] M.H. Jomroz, Vibrational Energy Distribution Analysis, VEDA4, Warsaw, 2004.
[27] G. Kereztury, S. Holly, J. Varga, G. Besenyei, A.Y. Wang, J.R. During, Vibrational spectra of monothiocarbomates-ii. IR and Raman spectra, vibrational assignment, conformational analysis and ab initio calculations of S-methyl-N,Ndimethylthiocarbamate, Spectrochim. Acta 49 (1993) 2007–2026.
[28] G. Keresztury, J.M. Chalmers, P.R. Griffith (Eds.), Raman Spectroscopy: Theory in Hand Book of Vibrational Spectroscopy, vol. 1, John Wiey &Sons Ltd, New York, 2002.
[29] J.S. Murray, P. Politzer, in: The Electrostatic Potential: an Overview, 1, Wiley Interdiscip Rev, 2011, pp. 153–163.
[30] B. Silvi, A. Savin, Classification of chemical bonds based on topological analysis of electron localization functions, Nature 371 (1994) 683–686.
[31] H. Jacobsen, Localized-orbital locator (LOL) profiles of transition-metal hydride and dihydrogen complexes, Can. J.Chem. 87 (2009) 695–973.
[32] W. Yang, R.G. Parr, Hardness, softness, and the fukui function in the electronic theory of metals and catalysis, Proc. Natl. Acad. Sci. U.S.A. 82 (1985) 6723–6726.
[33] T. Lu, F. Chen, Multiwfn: a multifunctional wavefunction analyzer, J. Comp. Chem. 33 (2012) 580–592.
[34] W Humphrey, A Dalke, K Schulten, VMD: visual molecular dynamics, J. Mol. Graph. 14 (1996) 33–38.
[35] G.M. Morris, R. Huey, W. Lindstrom, M.F. Sanner, R.K. Belew, D.S. Goodsell, A.J. Olson, Autodock4 and AutoDockTools4: automated docking with selective receptor flexiblity, J. Comput. Chem. 16 (2009) 2785–2791 2009.
[36] G.M. Morris, D.S. Goodsell, R.S. Halliday, R. Huey, W.E. Hart, R.K. Belew, A.J. Olson, Automated docking using a lamarckian genetic algorithm and empirical binding free energy function, J. Comput. Chem. 19 (1998) 1639–1662.
[37] P. Prusiner, M. Sundaralingam, The crystal and molecular structures of two polymorphic crystalline forms of virazole (1-p-D-Ribofuranosyl-l,2,4-triazole-3 carboxamide). A new synthetic broad spectrum antiviral agent, Acta Cryst. B32 (1976) 419.
[38] E.B. Wilson, J.C. Decius, P.C. Cross, Molecular Vibrations, Dover Publications Inc., New York, 1980.
[39] N.P.G. Roeges, A Guide to the Complete Interpretation of Infrared Spectra of Organic Structures, John Wiley and Sons Inc., New York, 1994.
[40] M. Snehalatha, C. Ravikumar, N. Sekar, V.S. Jayakumar, I. Hubert Joe, J. Raman Spectrosc 39 (2008) 928–936.

[41] V. Arjunan, S. Senthilkumari, P. Ravindran, S. Mohan, Synthesis, FTIR and FT-Raman spectral analysis and structure–activity relations of N-(4-bromophenyl)-2, 2-dichloroacetamide by DFT studies, J. Mol. Struct. 1064 (2014) 15–26.
[42] M.A. Al-Alshaikh, S. Muthu, E.S. Al-Abdullah, E. Elamurugu Porchelvi, S. Lahsasni, A.A. El-Emam, Macedonian J. Chem. Chem. Eng. 35 (1) (2016) 63–77.
[43] T. Rajamani, S. Muthu, Electronic absorption, vibrational spectra, non-linear optical properties, NBO analysis and thermodynamic properties of 9-[(2-hydroxyethoxy) methyl] guanine molecule by density functional method, Solid State Sci. 16 (2013) 90–101.
[44] I. Fleming, Frontier Orbitals and Organic Chemical Reactions, John Wiley & Sons, New York, 1976.
[45] M. Christophe, G. Andre, T.L. Alejandro, New dual descriptor for chemical reactivity, J. Phys. Chem. 109 (1) (2005) 205–212.
[46] P.K. Chattaraj, B. Maiti, U. Sarkar, Philicity: a unified treatment of chemical reactivity and selectivity, J. Phys. Chem. 107 (2003) 4973–4975.
[47] B. Delphine, M.P. Egloff, L. Mulard, C. Guerreiro, J.L. Romette, B. Canard, A structural basis for the inhibition of the NS5 Dengue virus mRNA 2-O-Methyl-transferase domain by Ribavirin 5-Triphosphate, J. Biol. Chem. 279 (34) (2004) 35638–35643.
[48] N. Yao, T. Hesson, M. Cable, Z. Hong, A.D. Kwong, H.V. Le, P.C. Weber, Structure of the hepatitis C virus RNA helicase domain, Nat. Struct. Mol. Biol. 4 (1997) 463–467.
[49] B. Gopal Samy, L. Xavier, Molecular docking studies on antiviral drugs for SARS, Int. J. Adv. Res. Comput. Sci. Software Eng. 5 (3) (2015) 75–79.